

基于磷酸盐玻璃微球腔的全光调谐光纤滤波器

陈彧芳, 沈骁, 周权, 张帅, 毛静怡, 万洪丹*

南京邮电大学电子与光学工程学院, 微电子学院, 江苏 南京 210023

摘要 提出并研究了一种基于磷酸盐玻璃微球腔的全光调谐光纤滤波器。利用自制的磷酸盐玻璃预制棒,以拉丝的方式制作出直径为 200~500 μm 、纤芯-包层折射率差为 0.004 的磷酸盐玻璃光纤。利用大功率 CO_2 激光器熔融加热光纤制备出 Q 值达 7.28×10^5 的微球腔。利用 1550 nm 波段的可调谐激光器,通过锥形光纤耦合方式激发微球腔内回音壁模式(WGM)共振,获得带宽约 2 pm、插入损耗小于 0.3 dB 的耦合共振谱。在不同功率泵浦光的注入下,磷酸盐玻璃微球腔具有比普通石英微球腔更高的光敏感特性。实验结果表明:当微腔泵浦光功率增加时,磷酸盐玻璃微球腔内的 WGM 共振谱向短波长漂移(蓝移),光热调谐灵敏度约为 72.727 pm/mW,线性度大于 0.99;在相同光功率变化下,普通石英微球腔内的 WGM 共振谱向长波长漂移(红移),光热调谐灵敏度约为 0.086 pm/mW,线性度较低。本文提出的磷酸盐玻璃微球腔全光调谐滤波器具有全光控制、结构紧凑、稳定性好、超窄带宽和调谐效率高等优势,在光纤传感和光纤通信等领域具有重要应用。

关键词 光纤光学; 磷酸盐玻璃; 微球腔; 全光调谐; 回音壁模式; 光热调谐

中图分类号 TN 248.1

文献标志码 A

doi: 10.3788/CJL202148.0106003

1 引言

可调谐光纤滤波器(TFF)以光纤为媒介,对传输光信号波长选择性地反射或透射,可作为光纤感应元件,亦可用于实现光纤激光器选模,在光纤传感和光纤通信中具有重要作用^[1-2]。早期的 TFF 主要包括马赫-曾德尔干涉仪(MZI)^[3-4]、光纤光栅^[5]、法布里-珀罗干涉仪(FPI)^[6-7]以及微结构干涉仪等^[8]。近几年,各种新结构、新材料的 TFF 及其在光传感和激光选模的应用成为了研究热点^[9-17]。2011年,Im等^[9]基于高双折射光子晶体光纤 Sagnac 型 TFF 实现激光选模,通过调节偏振控制器(PC)获得 12 nm 调谐范围的单波长或双波长激光输出。2012年,Kim等^[10]基于保偏光纤 MZI 型的 TFF,配合温控装置以及折射率匹配液,分别实现了 11.5 nm 和 6.54 nm 的波长调谐。2014年,Gao等^[11]提出一种微纳光纤 FPI 型 TFF,通过施加轴向应力实现灵敏度为 167.41 pm/mN 的机械调谐。

2014年,Yin等^[12]基于保偏-啁啾布拉格光栅(FBG)型 TFF,通过机械拉伸保偏-啁啾 FBG,实现调谐范围为 250 pm 的单纵模激光输出。2017年,Huang等^[13]在锥形微管中嵌入电热合金(FeCrAl)形成微腔型 TFF,实现了 0.57 nm 的电热调谐。2018年,本课题组^[14]将锥形保偏光纤与 PC 结合形成 Lyot 型 TFF,通过调节机械挤压式 PC,实现波长可调范围为 41.7 nm 的单/多波长调谐激光输出。2019年,Li等^[15]基于少模光纤与微球腔间的准临界耦合条件,实现机械频率调谐范围达 10^8 Hz 量级的 TFF;Tang等^[16]提出基于多模干涉型 TFF 的全光纤参量振荡器,通过机械调谐方式,实现 1494~1501 nm 和 1638~1629 nm 的双边带波长连续可调谐输出;Mao等^[17]基于亚波长光栅结构,通过微流控技术,实现波长可调范围达 28 nm 的 TFF。

上述 TFF 采用拉伸、扭转、温控等方法实现波长调谐,需要额外的机械或加热装置,结构相对复杂^[18]。2017年,Tian等^[19]利用外垂直入射泵浦光

收稿日期: 2020-07-06; 修回日期: 2020-07-22; 录用日期: 2020-08-18

基金项目: 国家自然科学基金青年科学基金(11704199)、江苏省研究生创新基金(KYCX19_0957、KYCX19_0963)、南京邮电大学大学生科技创新训练计划

*E-mail: hdwan@njupt.edu.cn

直接作用于石墨烯膜与微环微腔夹层结构,实现 0.78 nm 宽的共振波长全光调谐。2019 年, Yu 等^[20]提出微纳光纤耦合器结合 Sagnac 环的全光 TFF,实现的波长调谐灵敏度为 1 pm/mW。同年, Liu 等^[21]基于级联光-机械微环谐振器的全光 TFF,实现的波长调谐灵敏度为 43 pm/mW。2020 年,本课题组^[22]提出一种基于稀土光纤双花生结构微腔 MZI 型全光 TFF,实现了调谐范围为 12.36 nm 的单波长激光输出。

上述 TFF 通过结构简单、全光可控方法实现了波长调谐。光纤微腔作为一种特殊的微纳光纤器件,其具有高 Q 值、小模式体积、强光与物质相互作用以及高能量密度的特点,腔内回音壁模式(WGM)共振谱具有超窄带特性^[23]。结合特殊材料的光纤微腔,是实现窄带、可调谐滤波的高性能器件^[24-26]。2013 年, Ioppolo 等^[24]在石英微球腔表面镀 PDMS 膜,通过电场控制实现了 1.9 pm 的 WGM 波长调谐。2016 年, Ward 等^[25]提出了一种表面包覆稀土掺杂玻璃的毛细管微腔,通过毛细管内填充液体的温控方法,实现了腔内模式热调谐,获得了频率可调范围 > 70 GHz 的激光输出。2017, Yang 等^[26]提出一种表面涂覆掺铈溶胶-凝胶的有源微泡腔,实现了 240 pm 的 WGM 波长调谐。研究基于新型材料的 WGM 微腔,对于实现高灵活性、超窄带的全光可控 TFF 具有重要意义。

本文提出一种基于磷酸盐玻璃微球腔(PGMS)的全光 TFF。利用磷酸盐玻璃材料的强光敏感特性结合微球腔的高能量密度和窄带共振谱特性,实现了 WGM 的全光可调谐。通过自制的磷酸盐玻璃预制棒制备磷酸盐玻璃光纤,基于大功率 CO₂ 激光器熔融加热光纤制备出高 Q 值 PGMS。通过锥形光纤耦合方式激发微球腔内 WGM 共振。在不同功率泵浦光注入下,磷酸盐玻璃微球腔的光敏感特性远高于普通石英光纤微球腔,其 WGM 共振谱的漂移方向与普通石英微球腔相反。实验结果表明:当微腔泵浦光功率增加时,PGMS 的 WGM 共振谱向短波长(蓝移)漂移,光热调谐灵敏度最大约 72.727 pm/mW,线性度 > 0.99;在相同光功率变化下,WGM 共振谱向长波长漂移(红移),光热调谐灵敏度仅约为 0.086 pm/mW,线性度 < 0.7。该 PGMS 全光 TFF 具有全光纤、结构紧凑、稳定性好、超窄带宽和调谐效率高等优势,在光纤传感和光纤通信等领域具有良好的应用前景。

2 器件制备与工作原理

2.1 磷酸盐玻璃光纤的制备

通过预制棒拉丝法制备磷酸盐玻璃光纤。预制棒为磷酸盐玻璃材料(其材料体系主要为: P₂O₅-Na₂O-BaO-Al₂O₃-Nb₂O₅-Sb₂O₃-La₂O₃),经过高温熔制、搅拌,再出料浇注退火并使材料缓慢冷却至室温等流程制备。由于磷酸盐玻璃熔体与水有强烈的亲和力,并且以羟基基团的形式与玻璃结构结合,熔制玻璃时需采取通入 O₂ 和 CCl₄ 的方式进行除水处理(氧气的流量控制为 0.6 L/min,液态 CCl₄ 加热至 72 °C),保证除水充分反应,形成纤芯、包层激光玻璃样品。最后结合打孔、研磨、抛光、切割等工艺,分别实现纤芯和包层预制棒的制备。

利用预制棒拉丝制备磷酸盐玻璃光纤时,需要满足包层玻璃和纤芯玻璃的转移温度(T_g)匹配以及包层玻璃和纤芯玻璃热膨胀系数相近两个条件。拉丝装置主要包括送棒机构、加热炉、热电偶、拉丝滚轮等。具体拉丝过程为:1)将预制棒固定在送棒机构上,置于加热炉口中心并使之与地面保持垂直,实现均匀加热;2)操纵拉丝塔温度控制台,使温度升温至 575 °C,步长设置为 5~20 °C,保温时间约 10 min;3)待拉丝温度稳定之后,调整送棒速度以及最大送棒长度,同时利用拉丝系统控制拉丝速度(1.5~20 m/min)。其中,加热炉中电阻丝是整个拉丝塔的加热装置,负责加热预制棒;热电偶负责监测温度,以保证加热炉温度的稳定;拉丝滚轮是拉丝系统的核心,通过滚轮转速控制所制备光纤直径的大小。图 1 为预制棒拉丝法制备的磷酸盐玻璃光纤成品图。光纤直径在 200~500 μm 之间,其纤芯、包层折射率分别为 1.530 和 1.526,直径比为 1:2。



图 1 磷酸盐玻璃光纤成品

Fig. 1 Photo of the fabricated phosphate glass fiber

2.2 磷酸盐玻璃微球腔的制备

通过 CO₂ 激光器加热熔融磷酸盐玻璃光纤,基于表面张力效应制备 PGMS。图 2(a)为 CO₂ 激光器的准直聚焦系统,由 CO₂ 激光器、准直透镜、三维

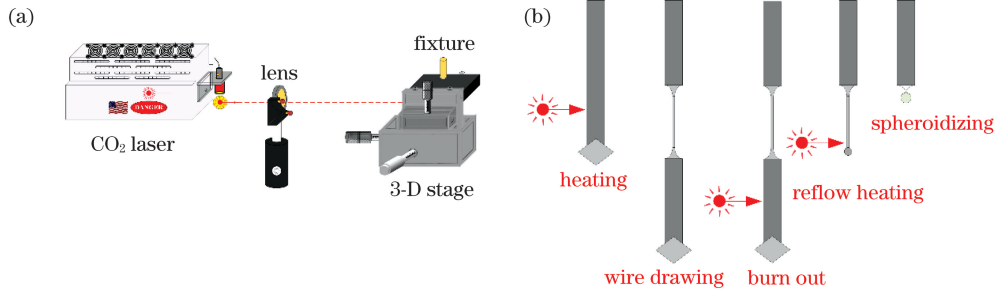


图 2 PGMS 的制备。(a)CO₂ 激光器的准直聚焦系统;(b)制备流程

Fig. 2 Preparation of PGMS. (a) Collimating and focusing system of CO₂ laser; (b) fabrication process

精密调节光纤架构成。图 2(b)为 PGMS 的制备流程,主要包括:1)将一段去除涂覆层的磷酸盐玻璃光纤用酒精擦拭干净然后固定于三维精密调节光纤架上;2)将 CO₂ 激光器光斑聚焦于磷酸盐玻璃光纤上,同时控制输出激光功率;3)利用高分辨率显微镜观察加热熔融玻璃光纤处直径尺寸的变化,实现熔融拉丝;4)调节激光器输出功率大小,向上持续移动玻璃丝尾端并加热熔融,形成 PGMS。图 3(a)为实验制备 PGMS 的实物照片,半径大小约为 78.91 μm。

2.3 锥形光纤的制备

图 3(b)为实验制备的普通单模锥形光纤的显微镜实物照片,单模光纤拉锥前直径大小为 125 μm,拉锥后直径大小约为 1.885 μm。实验中利用氢氧火焰加热熔融拉锥技术,严格控制拉锥速度和氢气流量,制备出损耗低、尺寸优良的锥形光纤。为实现光纤与 PGMS 的低损耗耦合,实验制备(拉锥速度 160 μm/s,拉锥长度 35000~37000 μm)的锥形光纤的锥区直径 < 2 μm,损耗 < 0.2 dB。

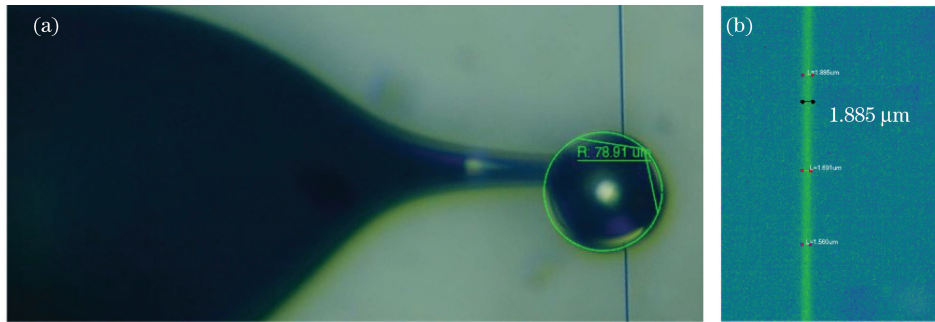


图 3 显微镜实物图。(a)磷酸盐玻璃微球-锥形光纤耦合;(b)锥形光纤

Fig. 3 Microscope images. (a) Couple of PGMS-tapered fiber; (b) tapered fiber

2.4 工作原理

当泵浦光以变化的功率进入 PGMS 时,光热效应使得微腔温度发生变化,由于热折变和热膨胀效应,微腔的折射率和尺寸发生变化,引起 WGM 共振波长漂移,具体可以表示为^[27]

$$n = n_0(1 + \xi\eta\Delta P) = n_0(1 + \xi\Delta T), \quad (1)$$

$$r = r_0(1 + \alpha\eta\Delta P) = r_0(1 + \alpha\Delta T), \quad (2)$$

式中:ξ 和 α 分别对应热折变与热膨胀系数;n₀ 和 r₀ 分别为微腔在注入泵浦光之前的折射率与半径

值;η 为温度与泵浦光功率之间的转换系数,取决于微腔的几何结构以及材料的吸收系数和热导系数;ΔT 和 ΔP 为微腔温度变化量和泵浦光功率变化量。微腔的 WGM 共振波长可以近似表示为

$$2\pi nr = m\lambda_0, \quad (3)$$

式中:m 为回音壁模式角模式数,λ₀ 为 WGM 共振波长。微腔共振波长的变化量 Δλ 与材料的热折变系数 ξ 和热膨胀系数 α 之间的关系为

$$\Delta\lambda = 2\pi r \cdot \frac{1}{m} \cdot \frac{dn}{dT} \cdot \Delta T + 2\pi nr \cdot \frac{1}{m} \cdot \frac{1}{r} \cdot \frac{dr}{dT} \cdot \Delta T = \lambda_0 \left(\frac{1}{n} \cdot \frac{dn}{dT} + \frac{1}{r} \cdot \frac{dr}{dT} \right) \cdot \Delta T = \lambda_0 \cdot (\xi + \alpha) \cdot \Delta T, \quad (4)$$

式中,当 PGMS 的温度变化量 $\Delta T > 0$ 时,热折变和热膨胀效应的响应时间不同,热折变效应的响应时间通常为几十微秒,而热膨胀效应的响应时间则远大于几十毫秒^[28]。因此,只考虑热折变效应条件下,引起 WGM 共振波长的蓝移。光热调谐灵敏度 S 可以表示为

$$S = \frac{d\lambda}{dP} = \frac{(\alpha + \xi)\lambda\eta}{1 - \frac{\lambda}{r} \frac{dr}{d\lambda} - \frac{\lambda}{n} \frac{dn}{d\lambda}} \quad (5)$$

由(5)式可知, ξ 、 α 越大, S 越高(一般玻璃材料, $\xi \gg \alpha$)。相比于普通的石英微球腔,本文提出的 PGMS 因具有较强的光热效应,且其 WGM 共振波长的全光调谐能力更强,可有效提高光热调谐灵敏度。

2.5 实验装置

锥形光纤的锥区直径与微腔内 WGM 光场的传播常数只有满足相位匹配条件才可以有效地激发 WGM 共振,从而实现高耦合效率的微腔-光纤耦合。同时,维持锥形光纤与磷酸盐微球腔表面的洁

净度,可获得高 Q 值、低插入损耗的 WGM 共振谱。图 3(b)为实验制备的 PGMS 与锥形光纤耦合的实物照片。图 4 为基于 PGMS 的全光 TFF 实验系统结构图,包括可调谐窄带激光器(TLS,线宽为 5 kHz、波长调谐范围为 120 nm、中心波长为 1550 nm)、可调光衰减器(VOA,可调范围为 0.5 dB~60 dB)、PC、微球腔-锥形光纤耦合单元、光电探测器(Photodetector,PD,带宽为 125 MHz,响应度为 40 V/mA)、反馈控制系统(Feedback,FB)以及由 TLS、耦合器(OC)和光功率计(OPM,分辨率为 0.001 dB)构成的功率监测系统。泵浦光依次经过 VOA、OC 以及 PC,调节泵浦光功率大小以及偏振态后,通过锥形光纤将光耦合进、耦合出 PGMS,利用三维位移平台精确控制微球腔与锥形光纤的耦合位置,通过高分辨率显微镜观测耦合过程。PD 接收输出信号并利用反馈控制单元的差分运算获得微球腔-锥形光纤的 WGM 共振谱。

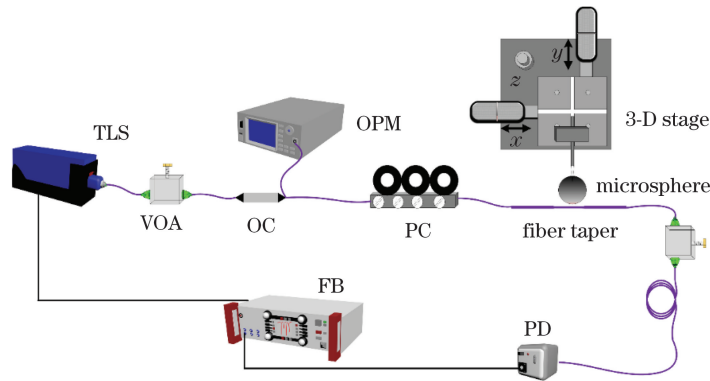


图 4 PGMS 的全光 TFF 实验系统装置示意图

Fig. 4 Experimental setup of the proposed all-optical TFF based on PGMS

3 实验结果与分析

3.1 磷酸盐玻璃微球腔的 WGM 共振谱测试

为提高耦合系统稳定性,采用过耦合的方法实现 PGMS 与锥形光纤的耦合,激发出 PGMS 的 WGM 共振谱。图 5 为实验测得的 WGM 共振谱。实验中可调谐激光器的调制波形为三角波,入射 PGMS 的光功率在 200 μW 附近。从图中可看出,WGM 共振波长在 1550.0700 nm 附近。由图 5 得到微球腔的 $Q = \frac{\lambda}{\Delta\lambda} = \frac{1550.0693}{0.00213} = 7.28 \times 10^5$,其中 λ 为共振波长, $\Delta\lambda$ 为共振峰的线宽。

3.2 小功率光热调谐性能测试

扫描 WGM 共振谱,研究瞬态过程中 PGMS 的光热调谐性能。WGM 扫描频率为 20 Hz(扫描

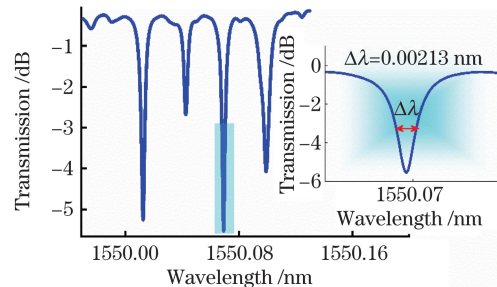


图 5 实验测得的 PGMS-锥形光纤的 WGM 共振谱

Fig. 5 Measured WGM resonance spectrum of the coupled PGMS-tapered fiber

速度为 5.6 nm/s)。首先测试泵浦光功率较小的 PGMS 的 WGM 共振谱变化规律,泵浦光功率变化范围为 500~900 μW ,保证其他条件不变。此外,系统在恒温环境下开展,实验平台加装了高精

密隔振装置,以确保实验结果稳定。图 6(a)为光功率逐渐增大情况下 WGM 共振波长漂移的测试结果,光谱未经过任何滤波处理,其中插图放大为共振波长在 1550.30 nm 附近的细节放大图。图 6(b)为 WGM 共振波长的漂移量与光功率的变化关系

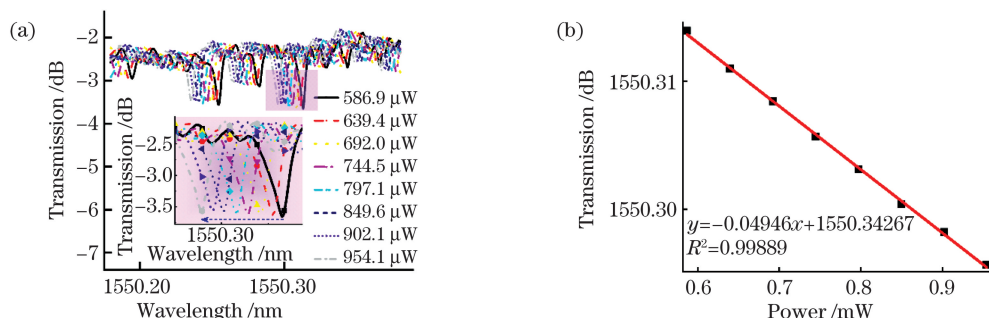


图 6 PGMS 的 WGM 共振谱随 μW 级光功率变化实验测试结果。(a)不同功率下的 WGM 共振谱;(b)WGM 共振波长漂移量随光功率的变化关系

Fig. 6 Experimental results of the WGM resonance spectra of microcavity varying with power (μW) for PGMS. (a) WGM resonance spectra measured under different power; (b) relationship between wavelength shift and optical power

3.3 大功率光热调谐性能测试

作为对比,继续增大泵浦光功率至 mW 量级,采用相同的方法测试全光调谐实验结果。泵浦光功率变化范围为 5.5~8.0 mW。图 7(a)为大功率条件下 WGM 共振波长漂移的测试结果图。图 7(b)为 WGM 共振波长的漂移量与光功率的变化关系图。从图中可以看出,PGMS 的 WGM 共振波长随光功率的增加向短波长(蓝移)漂移,最大漂移量约为 179.58 pm,光热调谐灵敏度约为 72.727 pm/mW,

图。实验结果表明,磷酸盐材料由于具有负的热折变系数^[29],其 WGM 共振波长随光功率的增加向短波长(蓝移)漂移,最大的漂移量约为 18.25 pm,光热调谐灵敏度约为 49.46 pm/mW,线性度 $R^2 > 0.99$ 。

线性度 $R^2 > 0.99$ 。通过对比图 7 与图 6,可知在不同光功率作用下,PGMS 的 WGM 共振谱漂移以及光热调谐灵敏度都会随着光功率的增大而增加。

图 7(c)和图 7(d)给出实验测试的普通石英微球腔($Q \approx 10^5$)内 WGM 共振谱随泵浦光功率的变化规律。根据(2)式,可知不同材料的热光系数和热膨胀系数不同,产生的光热效应也不同,上述因素均会对微腔光热调谐灵敏度产生直接影响。为了验证实验结果的有效性,采用相同的方法研究普通石英

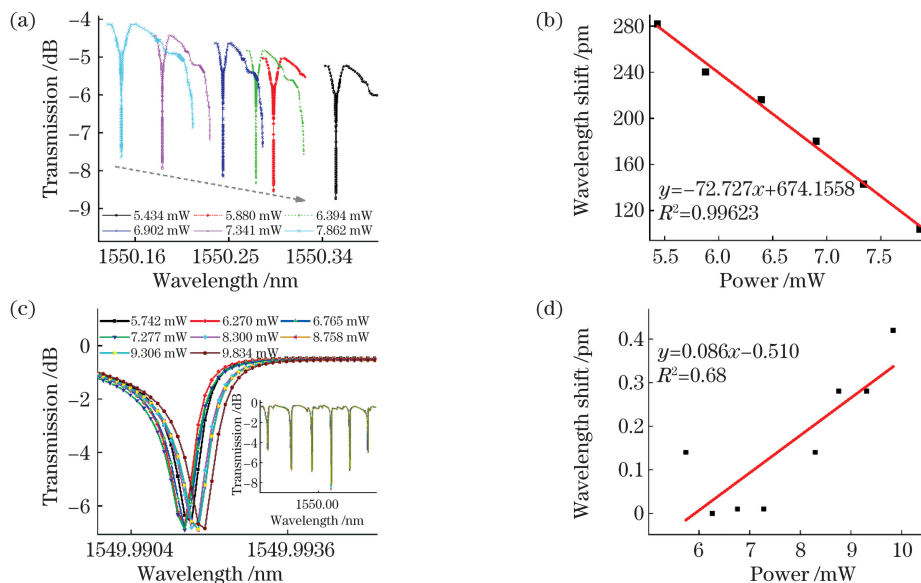


图 7 基于不同材料微球腔 WGM 共振谱随 mW 级光功率变化实验测试结果。(a)(b) PGMS;(c)(d)普通石英微球腔
Fig. 7 Experimental results of the WGM resonance spectra of microcavity varying with power (mW). (a)(b) PGMS; (c)(d) silica microsphere

微球腔的全光调谐特性。图 7(c)为光功率逐渐增大情况下 WGM 共振波长在 1549.99 nm 附近漂移的测试结果,插图为其完整的 WGM 共振谱。图 7(d)为 WGM 共振波长的漂移量与光功率的变化关系图。实验结果表明,石英材料由于具有正的热折变系数,其 WGM 共振波长随光功率增加向长波长(红移)漂移,最大漂移量约为 0.28 pm,光热调谐灵敏度仅有 0.086 pm/mW,且线性度 $R^2 < 0.7$ 。

实验过程中,严格控制光纤拉锥与拉丝工艺中的相关参数,如拉锥速度、氢气流量、CO₂ 激光器的输出功率大小等,可使微球与锥形光纤的尺寸可控。

表 1 不同类型光纤可调谐滤波器的性能比较

Table 1 Performance comparison of different optical fiber TFFs

Type of TFF	Q	Tuning method	Sensitivity or range of tuning
Sagnac filter with photonic crystal fiber ^[9]	—	Non-all-optical and mechanical	12 nm
In-line Mach-Zehnder ^[10]	—	Non-all-optical and temperature control	11.50 nm
In-line Fabry-Pérot ^[11]	—	Non-all-optical and mechanical	167.41 pm/mN
Microtube resonator ^[13]	3.10×10^4	Non-all-optical and electrical thermal	570 pm
Microring resonator ^[21]	—	All-optical	43 pm/mW
Ours	7.28×10^5	All-optical	72.727 pm/mW

4 结 论

提出一种基于 PGMS 的全光 TFF。通过自制的磷酸盐玻璃预制棒,制作直径为 200~500 μm、纤芯-包层折射率差为 0.004 的磷酸盐玻璃光纤。基于大功率 CO₂ 激光器熔融加热光纤制备出 Q 值为 7.28×10^5 的微球腔。利用中心波长为 1550 nm 的可调谐激光器,通过锥形光纤耦合方式激发微球腔内 WGM 共振,获得带宽约 2 pm、插入损耗 < 0.3 dB 的耦合共振谱。利用磷酸盐玻璃材料的强光热敏感特性结合 WGM 的高能量密度和窄带共振谱特性,实现了对磷酸盐微球腔的全光调谐特性测试。实验结果表明,当增加微腔泵浦光功率,PGMS 的 WGM 共振谱向短波长漂移(蓝移),光热调谐灵敏度最大约为 72.727 pm/mW,线性度 > 0.99 且稳定性好。普通石英微球腔在相同光功率变化下,WGM 共振谱向长波长漂移(红移),光热调谐灵敏度约为 0.086 pm/mW,且线性度较低。

参 考 文 献

[1] Peng S J, Liu Y N, Xue J L, et al. Design of multi-mode fiber tunable optical filter based on strain[J]. Chinese Journal of Lasers, 2011, 38(5): 0505004.

采用过耦合方法实现 PGMS 与锥形光纤的耦合,提高了耦合系统的稳定性,确保了实验的重复性。结果表明,通过控制 PGMS 以及锥形光纤的尺寸大小,光热调谐灵敏度的误差仅为 0.231 pm/mW,测试结果具有较高的一致性。

此外,将本文提出的基于磷酸盐玻璃微球腔的全光 TFF 的性能与之前报道过的不同类型的光纤可调谐滤波器进行比较,包括 Q 值大小、调谐方法以及调谐性能,结果如表 1 所示。磷酸盐玻璃微球腔的全光 TFF 基于较强的光热效应结合高 Q 值、高能量密度、窄线宽特性,可实现高达 72.727 pm/mW 的光热调谐灵敏度。

彭石军,刘亚南,薛金来,等. 基于应变的多模光纤可调谐光纤滤波器设计[J]. 中国激光, 2011, 38(5): 0505004.

- [2] Willner A E, Khaleghi S, Chitgarha M R, et al. All-optical signal processing [J]. Journal of Lightwave Technology, 2014, 32(4): 660-680.
- [3] Sun Y, Liu D, Lu P, et al. Dual-parameters optical fiber sensor with enhanced resolution using twisted MMF based on SMS structure [J]. IEEE Sensors Journal, 2017, 17(10): 3045-3051.
- [4] Wei L, Tatel G. Wavelength continuously tunable all-fiber flat-top comb filter based on a dual-pass Mach-Zehnder interferometer [J]. Journal of Lightwave Technology, 2019, 37(15): 3740-3749.
- [5] Dong X, Shum P, Ngo N Q, et al. A bandwidth-tunable FBG filter with fixed center wavelength [J]. Microwave and Optical Technology Letters, 2004, 41(1): 22-24.
- [6] Jia W H, Sun Q Z, Sun X H, et al. Microfiber Fabry-Perot filter consisting of two cascaded Sagnac reflectors for multi-wavelength fiber laser [J]. Proceedings of SPIE, 2013, 8924(5): 89242W.
- [7] Yu H, Luo Z, Zheng Y, et al. Temperature-insensitive vibration sensor with Kagomé hollow-core fiber based Fabry-Perot interferometer [J]. Journal of

- Lightwave Technology, 2019, 37(10): 2261-2269.
- [8] Han C Y, Zhao C Y, Ding H, et al. Spherical microcavity-based membrane-free FiZeu interferometric acoustic sensor [J]. Optics Letters, 2019, 44(15): 3677-3680.
- [9] Im J E, Kim B K, Chung Y. Tunable single- and dual-wavelength erbium-doped fiber laser based on Sagnac filter with a high-birefringence photonic crystal fiber [J]. Laser Physics, 2011, 21(3): 540-547.
- [10] Kim H J, Han Y G. Polarization-dependent in-line Mach-Zehnder interferometer for discrimination of temperature and ambient index sensitivities [J]. Journal of Lightwave Technology, 2012, 30(8): 1037-1041.
- [11] Gao S C, Zhang W G, Bai Z Y, et al. Microfiber-enabled in-line Fabry-Pérot interferometer for high-sensitive force and refractive index sensing [J]. Journal of Lightwave Technology, 2014, 32(9): 1682-1688.
- [12] Yin B, Feng S C, Liu Z B, et al. Tunable and switchable dual-wavelength single polarization narrow linewidth SLM erbium-doped fiber laser based on a PM-CMFBG filter [J]. Optics Express, 2014, 22(19): 22528-22533.
- [13] Huang D M, Huang W, Zeng J, et al. Electrical thermo-optic tuning of whispering gallery mode microtube resonator [J]. IEEE Photonics Technology Letters, 2017, 29(1): 169-172.
- [14] Yuan F, Zhao J J, Jiang W F, et al. Optical property of polarization-maintaining fiber taper for tunable multi-wavelength fiber laser generation [J]. IEEE Photonics Journal, 2019, 12(1): 1-9.
- [15] Li X T, Chang P F, Huang L G, et al. Feasibility of quasicritical coupling based on LP modes and its application as a filter with tunable bandwidth and stable insertion loss [J]. Optics Express, 2019, 27(16): 23610-23619.
- [16] Tang Z, Zhang J X, Fu S J, et al. Tunable CW all-fiber optical parametric oscillator based on the multimode interference filter [J]. Infrared and Laser Engineering, 2019, 48(5): 0520002.
唐钊, 张钧翔, 付士杰, 等. 基于 MMI 滤波器的可调谐连续光全光纤 OPO [J]. 红外与激光工程, 2019, 48(5): 0520002.
- [17] Mao Q, Tang X G, Meng F, et al. Tunable narrow-band filter with sub-wavelength grating structure by micro-optofluidic technique [J]. Laser & Optoelectronics Progress, 2019, 56(4): 042301.
毛强, 唐雄贵, 孟方, 等. 基于亚波长光栅结构的微流控可调窄带滤波器设计与分析 [J]. 激光与光电子学进展, 2019, 56(4): 042301.
- [18] Ma L, Qi Y H, Kang Z X, et al. Tunable fiber laser based on the refractive index characteristic of MMI effects [J]. Optics & Laser Technology, 2014, 57: 96-99.
- [19] Meng Y H, Deng L, Liu Z L, et al. All-optical tunable microfiber knot resonator with graphene-assisted sandwich structure [J]. Optics Express, 2017, 25(15): 18451-18461.
- [20] Yu Y, Bian Q, Wang J F, et al. All-optical modulation characteristics of a microfiber coupler combined Sagnac loop [J]. IEEE Photonics Journal, 2019, 11(1): 1-11.
- [21] Liu L, Xue W, Jin X, et al. Bandwidth and wavelength tunable all-optical filter based on cascaded opto-mechanical microring resonators [J]. IEEE Photonics Journal, 2019, 11(1): 1-10.
- [22] Wan H D, Chen Y F, Zhou Q, et al. Tunable, single-wavelength fiber ring lasers based on rare earth-doped, double-peanut fiber interferometers [J]. Journal of Lightwave Technology, 2020, 38(6): 1501-1505.
- [23] Liu K, He Y, Yang A, et al. Resonant response and four-wave mixing via microsphere coupled with microfiber coupler [C] // 2018 Asia Communications and Photonics Conference (ACP), October 26-29, 2018, Hangzhou, China. New York: IEEE Press, 2018: 18355856.
- [24] Ioppolo T, Ötügen V, Ayaz U. Development of whispering gallery mode polymeric micro-optical electric field sensors [J]. Journal of Visualized Experiments, 2013(71): e50199.
- [25] Ward J M, Yang Y, Chormaic S N. Flow sensor using a hollow whispering gallery mode microlaser [J]. Proceedings of SPIE, 2016, 9727: 972718.
- [26] Yang Y, Lei F C, Kasumie S, et al. Tunable erbium-doped microbubble laser fabricated by Sol-gel coating [J]. Optics Express, 2017, 25(2): 1308-1313.
- [27] Lin W, Zhang H, Liu B, et al. Laser-tuned whispering gallery modes in a solid-core microstructured optical fibre integrated with magnetic fluids [J]. Scientific Reports, 2015, 5: 17791.
- [28] Gensch T, Viappiani C. Time-resolved photothermal methods: accessing time-resolved thermodynamics of photoinduced processes in chemistry and biology [J]. Photochemical & Photobiological Sciences, 2003, 2(7): 699-721.
- [29] Jiang Z H. Optical functional glasses [M]. Beijing: Chemical Industry Press, 2008: 26-27.
姜中宏. 新型光功能玻璃 [M]. 北京: 化学工业出版社, 2008: 26-27.

All-Optical Tunable Fiber Filter Based on Phosphate Glass Microspheres

Chen Yufang, Shen Xiao, Zhou Quan, Zhang Shuai, Mao Jingyi, Wan Hongdan*

College of Electronic and Optical Engineering & College of Microelectronics, Nanjing

University of Posts and Telecommunications, Nanjing, Jiangsu, 210023, China

Abstract

Objective A tunable fiber filter (TFF) takes an optical fiber as the medium to realize wavelength-selective reflection or transmission of optical signals. TFFs play an important role in optical fiber sensing and communication owing to their inherent merits of anti-electromagnetic disturbance, compact size, and low fabrication cost. Compared with traditional interferometer TFFs, such as Mach-Zehnder interferometer, fiber Bragg gratings, Fabry-Perot interferometers, and microstructure interferometers, an optical fiber microcavity has a high quality factor, high energy density, and whispering-gallery mode (WGM) resonance spectrum with an ultra-narrow band. Moreover, research on WGM microcavities based on new materials is of great significance for realizing an all-optical controllable TFF with high flexibility and tunable filtering. An all-optical TFF with a simple structure can eliminate the need for applying additional mechanical devices or heating devices to realize dynamic tuning. In this paper, an all-optical TFF based on phosphate glass microspheres (PGMS) is proposed to facilitate a systematic study of optic-thermal tunability. With the advantages of all-optical control, compact structure, high stability, and ultra-narrow bandwidth, all-optical TFFs based on PGMS could be widely used in fiber sensing elements or mode selection of fiber lasers, providing good application prospects in the field of optical fiber communication.

Methods The components of a PGMS microcavity coupling system include the phosphate glass optical fiber (PGOF), PGMS and single mode tapered fiber. The PGOF was prepared by preform-drawing method. After high temperature melting, stirring, pouring, annealing and cooling to room temperature slowly, the optical fiber preforms of core and cladding were prepared, respectively. Then, the PGOF was fabricated by wire drawing with the preforms and then fused and stretched by CO₂ laser heating with a certain power. At the same time, the diameter changes of the PGOF were observed by high resolution microscope, and the microsphere was formed based on surface tension effect. The single mode tapered fiber with low loss and good size was tapered by controlling the cone drawing speed and hydrogen flow rate strictly. The sizes of PGMS and the single mode tapered fiber were characterized by optical microscope, including the diameter and waist width. According to the above preparations of three optical components, the WGM resonance spectrum with high Q value and low insertion loss was obtained by efficiently coupling PGMS with the single mode tapered fiber.

Results and Discussions The optic-thermal tunability of PGMS was studied by scanning WGM resonance spectrum under transient process. In the measurement of low power optic-thermal tuning, with the increase of optical pump power, the WGM resonance wavelength drifts to a shorter wavelength (blue shift). The maximum drift is about 18.25 pm and the optic-thermal tunable sensitivity is about 49.46 pm/mW with a linearity more than 0.99. In the test of high power optic-thermal tuning performance, the WGM resonance wavelength of PGMS drifts to the shorter wavelength (blue shift) with the increase of optical pump power. The maximum drift is about 179.58 pm and the optic-thermal tunable sensitivity is around 72.727 pm/mW with a linearity more than 0.99. According to the experimental results, the WGM resonance spectrum drifts and optic-thermal tuning sensitivity of PGMS increases with the increase of optical pump power. Furthermore, in order to verify the effectiveness of the experimental results, the all-optical tuning characteristics of the TFF based on silica microsphere were studied with the same method. The experimental results show that the WGM resonance wavelength of silica microsphere shifts to the longer wavelength (red shift) with the increase of optical pump power. The results of silica microsphere and PGMS are different, which depend on the characteristics of the material itself. The maximum drift is about 0.28 pm and the optic-thermal tunable sensitivity is only about 0.086 pm/mW with a linearity less than 0.7. By comparison, it can be seen that the all-optical TFF of PGMS based on strong optic-thermal effect combines with high Q value, high energy density and narrow linewidth characteristics, and achieves an optic-thermal tunable sensitivity up to 72.727 pm/mW.

Conclusions An all-optical TFF based on PGMS was proposed and demonstrated. Fabricate the microsphere with high Q value was fabricated using the high power CO₂ laser by melting and heating the fiber. The microsphere was

coupled efficiently by a single mode tapered fiber and the WGM resonance was excited by a tunable laser source. With a varied optical pump power, the PGMS has higher optical sensitivities than the silica microsphere. As for the PGMS, an increased pump power results in WGM resonance wavelength shifting to a shorter wavelength (blue shift), and the optic-thermal tunable sensitivity is about 72.727 pm/mW with a high linearity of >0.99 . However, in the same condition, the WGM resonance wavelength of the silica microsphere shifts to a longer wavelength (red shift), and the optic-thermal tunable sensitivity is only about 0.086 pm/mW with a much lower linearity. The proposed all-optical TTF based on PGMS has the advantages of all-optical control, compact structure, high stability, ultra-narrow bandwidth and highly tunable efficiency, which will be used widely in the field of power system, optical fiber sensing and optical fiber laser.

Key words fiber optics; phosphate glass; microsphere; all-optical tunability; whispering gallery mode; optic-thermal tunability

OCIS codes 060.2310; 140.3945; 160.5690; 230.1150